A New Viscoelastic Phase-Transformation Model to Simulate the Injection-Molding Residual Stress

SHIH-JUNG LIU

Department of Mechanical Engineering, Chang Gung College of Medicine and Technology, Kwei-San, Tao-Yuan 333, Taiwan, Republic of China

SYNOPSIS

The focus of this study is on thermally induced residual stress, which is the predominant cause for dimensional imperfections in unfilled injection-molded plastic products. A new viscoelastic phase-transformation model was proposed to simulate and predict the residual stress within injection-molded articles as induced during the cooling stage of the injection-molding cycle. The calculated results are in good agreement with the literature experimental data. Numerical simulation of a residual stress problem can be used to guide corrective measures if the problem arises and also to prevent a potential problem from occurring in the first place. © 1996 John Wiley & Sons, Inc.

INTRODUCTION

Injection molding is one of the most important polymer processing methods for producing plastic parts.[1] However, there are still several unresolved problems that confound the overall success of the injection-molding process, the product's residual stress caused by inappropriate mold design and processing conditions being one of them. To predict well the residual stress in a polymer product, one must account for the effect of the processing conditions, the material behavior, and the geometric effects.

As injection molding is a complex process, a number of factors can affect the dimensional requirements of the product. A good understanding of the process can assist the product and mold designer to anticipate and avoid the development of the product's residual stress with the origins in the following three segments of the injection-molding cycle: (1) filling, (2) packing/holding, and (3) cooling. In essence, both the thermal expansion coefficient and the stiffness of the material, coupled to the transient temperature gradient within the material, drives the formation of the thermally induced residual stresses. The incomplete relaxation of the flow-induced stresses (which arises during the filling and packing/holding stages of the molding cycle) may also contribute to the final stress field within the solidified article, but their residual stress effects tend to be relatively small for typical small-size injection-molding articles. Flow-related effects can, however, influence the nature of thermally induced residual stresses in that anisotropic thermal and mechanical properties are a consequence of the velocity gradients within the mold cavity. Furthermore, the initial temperature field within the cavity for the onset of cooling is established during the mold-filling process. As such, the processing conditions, i.e., both the velocity gradients and the temperature gradients, are potentially important factors to consider while modeling the residual stress of injection-molded parts. Other factors that affect the final residual stress of injection-molded parts are the thermophysical properties such as the thermal expansion coefficient, heat conductivity, heat capacity, and material density which are functions of the temperature. For semicrystalline materials, the crystalline enthalpy of the cooling exotherm will also affect the material properties, which, in turn, influence the residual stresses.

To investigate the effects of residual stresses on the dimensional integrity of injection-molded parts, several experimental methods have been used to measure the residual stresses. One of these methods

Journal of Applied Polymer Science, Vol. 62, 1537–1550 (1996)
 CCC 0021-8995/96/101537-14

is the layer-removal technique.[2] So and Broutman[3] used this method to measure the residual stresses in quenched polycarbonate and acrylic plates. They also investigated the effect of residual stresses on the impact strength of injection-molded parts and concluded that the residual stresses could lead to plastic yielding in bending experiments. Cuckson et al.[4] used the same technique to measure the stress distributions within thick-section injection-molded parts and concluded that it was not possible to produce an accurate through-thickness stress profile within the thick parts. Mandell et al.[5] used the method to measure the residual stress distributions within injection-molded polysulfone, and they also related the residual stress profiles to the fatigue and crack of the molded, quenched, and annealed parts. Siegman et al.[6] used the technique to relate the effect of melt temperature, mold temperature, injection rate, and injection pressure on the final residual stress profiles. All these effects might vary the state of residual stress in molded amorphous plastics from compressive stress at the surface and tensile at the interior to tensile at the exterior and compressive within the core layer. Isayev and Crouthmel[7] also used this scheme to find the residual stresses in a quenched plate and compared their experimental data with predicted results obtained from two different models. Thompson and White[8] used the layer-removal scheme to measure the residual stress distributions within molded and annealed bars. Hornberger and DeVries[9] also used this scheme to examined the effect of residual stresses on the mechanical properties of a polycarbonate bar. Their findings revealed that quenching of the polycarbonate would increase the fatigue strength by a factor of about 10. Iacopi and White[10,11] used the layer-removal method and fatigue tests to examine the residual stresses and aging effects in injection-molded polystyrene and polycarbonate parts. Hastenberg et al.[12] used a modified layer-removal scheme to measure the thermal stresses in a compression-molded part and studied the effect of pressure history on the final residual stress profiles. Thakkar et al.[13] used the layer removal scheme to examine the effect of cold working and residual stress in polycarbonate bars. Finally, Hindle et al.[14] used a layer-removal technique to examine the internal stresses and molecular orientation. They also employed a Moir shadow fringe pattern to study the distortion of injection-molded polypropylene and glass fiber-reinforced polypropylene.

Another method that is frequently used to evaluate the residual stress profiles utilizes the photoelastic technique of measuring the optical birefringence.[2] Broutman and Krishmakumar[15] used birefringence measurements to examine the residual stresses and the relationship between the thermal treatment and the impact strength of several polymers. Kamal and Tan[16] also used this method to study the development of frozen-in stresses within an injection-molded polystyrene. They found that the relaxation phenomena are not very important during the filling stage but become more important for the packing/holding stages. Saffell and Windle[17] used a modified method to separate the elastic stresses (thermally induced) from the overall birefringence patterns. They concluded that the elastic stresses relaxed considerably via annealing whereas the birefringence did not (i.e., the flow-induced effects remained largely unchanged). Wust and Bogue[18] used the photoelastic scheme to evaluate the residual stresses within quenched polystyrene plates. Isayev[19] also used birefringence measurement to evaluate the distributions within injection-molded polystyrene bars and in quenched polystyrene and acrylic bars. Their discussions included the effects of processing condition, bar thickness, and runner diameter on the development of orientation. Takeshima and Funakoshi[20] used birefringence, heat shrinkage, and laser-Raman spectroscopy to measure the molecular orientation distribution within injection-molded polycarbonate discs. They concluded that the pattern within the disk revealed three different molecular orientation zones: a skin zone in contact with the mold, a core zone located at the center, and a shear zone between the skin and the core zones. Mittal and Rashmi[21] also used this method to measure the residual stresses in circular acrylic rods. They concluded that both flow-induced stresses and thermally induced stresses lead to the development of molecular orientation. Lee et al.[22] measured the effects of sample size and initial temperature on the residual stresses profiles. Mittal and Rashmi[23] used the photoelastic technique to find the effect of thermal history on the distribution of residual stresses as well as molecular orientations within acrylic rods. Chan and Lee[24] used this method to correlate processing conditions such as draw ratio, cooling rate, die temperature, melt temperature, and die gap with the final molecular orientation and internal stresses within extended polypropylene sheets. Finally, Flaman[25,26] used the same technique to study the buildup and relaxation of molecular orientation, residual stress, and density distributions within injection-molded parts.

Compared to the research efforts on the experimental investigations, not as much work has been done in the area of residual stress simulation. Lee

et al.[27,28] were among the first to propose a thermorheologically simple viscoelastic model that predicted the stresses in a glass plate cooled symmetrically from both surfaces. They used measured relaxation functions combined with a finite difference scheme to complete the model, known as the Lee, Roger, and Woo (LRW) model, which is a Maxwell model subjected to small strains. Aggarwala and Saibel[29] predicted the residual stresses using a simpler model, which proved to be a reduction of the LRW model by assuming rheological behavior in which the relaxation was zero above some critical temperature T_g and a large constant below the T_g. Narayanaswamy and Gardon[30] used the LRW viscoelastic model to predict the residual stresses in tempered glass. Ohlberg and Woo[31] performed the thermal stress analysis of glass with the temperature-dependent thermal expansion coefficient being represented by a hypertangent function. Struik[32] discussed the formation of cooling stresses in amorphous polymers and the importance of including the phase transformation as part of the simulation for the cooling-induced stresses within injection-molded parts. Frutiger and Woo[33] used the LRW equations to carry out a thermoviscoelastic analysis for circular plates modeled with thermorheologically simple materials. A Dirichlet series was used in their analyses to approximate the basic Maxwell model so that the generalized Maxwell model was obtained. Mills[34] used a model based on the equations proposed by Aggarwala and Siebel to predict the residual stresses in plastics, rapidly cooled from the melt. Maneschy et al.[35] completed the residual stress analysis of an epoxy plate subjected to rapid cooling on both surfaces using the LRW model. Tamma et al.[36,37] calculated the stress response in injection-molded articles via a transfinite element scheme. Cohen and Dibbs[38] studied the interaction between heat transfer, shrinkage, and stress relaxation during postforming cooling of thermoplastic materials. Douven[39] proposed a viscoelastic model to predict the residual stresses in injection-molded parts. Rezayat and Stafford[40] proposed a transversely isotropic viscoelastic model which is an exclusive derivation of the LRW model to analyze anisotropic injection-molded parts. Finally, Baaijens[41] used a viscoelastic phase transformation based on the Maxwell model to simulate the formation of flow and thermally induced residual stresses in injection-molded products. Both Douven and Baaijens concluded that the use of free boundary conditions along the length direction leads to a tensile residual stress at the core and compressive stresses near the surfaces when modeling an injection-molded part. However, the use of constrained boundary conditions along the length direction leads to tensile stresses at the core, compressive stresses at the outer layers, and tensile stresses very near the surfaces.

The focus of this article was on the modeling and simulation of thermally induced residual stress for injection-molded parts. A new viscoelastic phase-transformation model incorporating a 2-D overlay finite element scheme was proposed to simulate the injection-molded residual stress. The numerical simulation will provide an improved understanding of the induced residual stress inside plastic articles.

THEORY OF VISCOELASTIC PHASE-TRANSFORMATION MODEL

A new viscoelastic phase-transformation model is proposed to simulate the thermally induced stress of injection-molded articles. The model accounts for the viscoelastic behavior of the polymer in its solid state and assumes that the behavior of unsolidified polymer follows that of a viscous fluid. In the analysis of a nonlinear problem, it is always assumed that the total strain rate, $\dot{\varepsilon}$, is separable into an elastic, $\dot{\varepsilon}_e$, component, and a viscoplastic, $\dot{\varepsilon}_{vp}$, component, i.e., $\dot{\varepsilon} = \dot{\varepsilon}_e + \dot{\varepsilon}_{vp}$. The total stress rate depends on the elastic strain rate according to

$$\dot{\sigma} = [D]\dot{\varepsilon}_e \tag{1}$$

where $[D]$ is the elasticity matrix. The onset of viscoplastic behavior is governed by the yield criterion $F(\sigma, \varepsilon_{vp})$, which is a function of stress and viscoplastic strain rate. If F is larger than the uniaxial Von Mises yield stress σ_y, the viscoplastic flow occurs. Here, we use the specific viscoplastic flow constitutive equation recommended by Liu and Rietveld[42] where the viscoplastic strain rate depends only on the current stresses given as

$$\dot{\varepsilon}_{vp} = \frac{1}{3\eta}\langle \Phi(F) \rangle \frac{\partial F}{\partial \sigma} \tag{2}$$

where η is the viscosity and $\Phi(F)$ is the strain rate function which can be represented as

$$\langle \Phi(F) \rangle = \Phi(F) \quad \text{for } F > \sigma_y \tag{3a}$$

$$= 0 \quad F < \sigma_y \tag{3b}$$

with the functions Φ and F defined by

$$\Phi(F) = F - \sigma_y \tag{4}$$

$$F = (3tr\sigma'^2)^{1/2} \tag{5}$$

where σ' is the deviatoric stress tensor. Equation (2) can be rewritten as

$$\dot{\varepsilon}_{vp} = \frac{1}{2\eta}\left\langle 1 - \frac{\sigma_y}{(3tr\sigma'^2)^{1/2}}\right\rangle \sigma' \tag{6}$$

An examination of the specific characteristics of eq. (6) in certain limiting cases will determine the range over which this constitutive equation is applicable. First, when the yield stress σ_y is zero in eq. (6), the total strain rate $\dot{\varepsilon}$ is given by

$$\dot{\varepsilon} = \frac{(1+\upsilon)}{E}\dot{\sigma} - \frac{\upsilon}{E}(tr\dot{\sigma})I + \frac{1}{2\eta}\sigma' \tag{7}$$

where the first two terms on the right-hand side represent the elastic strain rate and the third term represents the viscous strain rate. When the elastic component of the shearing deformation is small enough compared with the viscoplastic component, the Newtonian fluid model can be obtained from eq. (7) as follows:

$$\sigma = 2\eta\dot{e} - \tfrac{2}{3}\eta(tr\dot{\varepsilon})I + \tfrac{1}{3}(tr\sigma)I \tag{8}$$

Furthermore, when the elastic volume dilatation term $(tr\dot{\varepsilon})$ is removed from eq. (8), we have

$$\sigma = 2\eta\dot{e} + \tfrac{1}{3}(tr\sigma)I \tag{9}$$

which is the model for an incompressible Newtonian fluid. Another limiting case of importance is when the viscosity η in eq. (7) is infinite or a very large number; the current elasto-viscoplastic model reduces to the linear elastic model.

With the viscoplastic strain defined by eq. (6), the strain increment $\Delta\varepsilon_{vp}^n$ occurring during the time step $\Delta t^n = t^{n+1} - t^n$ is given by

$$\Delta\varepsilon_{vp}^n = \Delta t^n[(1-\Theta)\dot{\varepsilon}_{vp}^n + \Theta\dot{\varepsilon}_{vp}^{n+1}] \tag{10}$$

The fully explicit scheme, i.e., $\Theta = 0$ in eq. (10), was used for the strain increment calculation. The numerical implementation starts from the following equilibrium equation:

$$\int_V [B^n]^T\sigma^n dV + f^n = 0 \tag{11}$$

where f^n is the vector of equivalent nodal thermal loads and the superscript n denotes a time dependence. With some derivation, an initial stiffness matrix of the form

$$[K^n] = \int_V [B^n]^T[D^n][B^n]dV \tag{12}$$

is obtained, which leads to the following equation ready for solving:

$$[K^n]\{\Delta d\}_m = \int_V [B^n]^T[D^n]\dot{\varepsilon}_{vp}^n\Delta t^n dV + \Delta f^n \tag{13}$$

After determining the displacement at every step, the stress and strain are obtained via the following expressions:

$$\{\Delta\varepsilon\}_m = [B]^T\{\Delta d\}_m \tag{14}$$

$$\{\Delta\sigma\}_m = [D]\{\Delta\varepsilon - \Delta\varepsilon_{vp} - \Delta\varepsilon_0\}_m \tag{15}$$

$$\sigma_{m+1} = \sigma_m + \Delta\sigma_m \tag{16}$$

The stress is then obtained which will be used to calculate the strain rate and the relative pseudo load for the next time step. As time proceeds and the part cools down, the residual stress will be obtained.

To expand the applicability of this viscoelastic phase-transformation model, we adopt the overlay finite element scheme.[43] The polymer to be analyzed is modeled as a composite of "side-by-side" layers. Each layer can have a different "thickness" and exhibit different material behavior. The "thickness" here is not a real thickness in a physical sense or in the finite element scheme; instead, it is a mathematical way of representing different overlays within a control volume. The nodes that are coincident undergo the same amount of deformation. The total stress field is obtained by summing the different contributions from each overlay. Because the mechanical behavior of each overlay is different, it contributes to the total stress field according to the dimensionless thickness of each overlay, tj, so that

$$\sigma = \sum_{j=1}^{k}\sigma_j t_j \qquad \sum_{j=1}^{k} t_j = 1 \tag{17}$$

where k is set to two here (i.e., two layers) and the thickness in each layer is $t_1 = t_2 = \frac{1}{2}$ in the analysis. The equilibrium equation [eq. (11)] becomes

$$\int_v [B^n]^T\left(\frac{\sigma_1^n + \sigma_2^n}{2}\right)dV + f^n = 0 \tag{18}$$

The element stiffness matrix given by eq. (12) is now the sum of each overlay contribution as follows:

$$[K^n] = \int_v [B^n]^T([D^n])_1[B^n]dV + \int_V [B^n]^T([D^n])_2[B^n]dV \tag{19}$$

Finally, eq. (13) becomes the sum of different overlay contributions so that the behavior of a complex material can be evaluated via

$$[K^n]\{\Delta d\}_n = \int_V [B^n]^T([D^n]\dot{\varepsilon}_{vp}\Delta t^n)_1 dV + \int_V [B^n]^T([D^n]\dot{\varepsilon}_{vp}\Delta t^n)_2 dV + \Delta f^n \tag{20}$$

where the subscripts 1 and 2 denote the contributions from the two different layers.

The viscoelastic analysis begins from the original six-parameter combination achieved by overlaying two three-parameter (E, η, σ_y) models. To obtain the standard linear solid model, we set zeros to the two yield stresses. Then, one of the viscosities is set to be a very large number (10^{20} or even larger). The combination behaves as a parallel connection of a Maxwell element and a linear elastic element, which is the standard linear solid model. On the other hand, by assigning zeros to the two yield stresses and very large numbers to the two elastic modules, the viscous fluid properties were displayed. Therefore, this viscoelastic model can be formulated from a standard linear solid to a viscous fluid, which captures the phase-transformation behavior, with viscous behavior in any unsolidified regions and viscoelastic behavior in any solidified regions.

For the explicit scheme used here, the stable time criterion derived by Cormeau[44] with a Von Mises yield criterion and a zero yield stress was utilized. The stability criterion has the following form for linear function $\Phi(F) = F$:

$$\Delta t \leq \frac{4(1 + \nu)\eta}{3E} \tag{21}$$

If an implicit scheme is used for the simulations, the maximum time limit for the stable iterations can be avoided. However, the implicit scheme increases the computational time by a factor of approximately 4–5 in comparison with the explicit approach, because to perform the calculation requires the reformation of the stiffness matrix for the same time step length. Besides, if the time step length used is too large, the result will deteriorate. For the current study, the time length limit for the explicit scheme is long enough, which makes this method more favorable to use. In the numerical application, a variable time step scheme was used which amounted to the combination shown in eq. (22) where a variant is used to limit the time step length[43]:

$$\Delta t_m \leq \left\{\left[C_1\left[\frac{\varepsilon_{ii}^m}{(\dot{\varepsilon}_{ii})_{vp}^m}\right]^{1/2}\right]\right\}_{\min} \tag{22}$$

In eq. (22), ε_{ii}^m is the first total strain invariant and $(\dot{\varepsilon}_{ii})_{vp}$ is the first viscoelastic strain rate invariant. The minimum in eq. (22) is that taken over all integrating points in the control volume. The value of the constant C_1 is specified as 0.11 for explicit time marching schemes.[43] Another useful limit that can be imposed while using the variable time stepping scheme is that the change in the time step length falls between any two intervals as limited by

$$\Delta t_{m+1} \leq C_2 \Delta t_m \tag{23}$$

where C_2 is a constant of value 1.5.[43] However, the most important time limit during the calculation is the one discussed earlier which was derived by Cormeau. Every time step for all iterations needs to be smaller than the maximum allowable time length Δt discussed earlier, i.e.:

$$\Delta t_m \leq \Delta t = \frac{4(1 + \nu)\eta}{3E} \tag{24}$$

TRANSIENT HEAT-TRANSFER ANALYSIS

As the polymeric material cools inside the mold cavity, the calculation of thermally induced residual stresses within the solidifying material first requires the transient temperature gradients to be evaluated. It is the temperature changes that cause a residual stress profile to develop, and the transient temperature field also determines the location of the solid–liquid interface during the phase transformation. Since most injection-molded parts are relatively thin compared to their surface area and also because of the high thermal conductivity of the metal mold which surrounds the poorly conducting polymer, the

removal of heat from the polymer during an injection-molding process largely occurs via heat conduction in a direction perpendicular to plane of the part. It is also commonly assumed that during cooling the polymer within the mold remains in contact with the mold walls. The thermal contact resistance during the injection-molding cooling process from the relatively small gap[45] is neglected here and its influence on the residual stress will be discussed in future articles. The heat-transfer analysis begins from the heat-conduction equation with assigned temperatures on the boundaries of the system:

$$\rho C_p \frac{dT}{dt} = k\nabla^2 T \tag{25}$$

where ρ is the density; C_p, the heat capacity; and k, the thermal conductivity of the polymer. By introducing the finite difference discretization for eq. (25), we can get the following equations for iteration:

$$([C] + \Theta\Delta t[K])\{T\}^{t+\Delta t} = ([C] - (1-\Theta)\Delta t[K])\{T\}^{t} \tag{26}$$

with

$$[K] = \int_V [B]^T k[B]\, dV$$

$$[C] = \int_V [N]^T \rho C_p[N]\, dV$$

$\Theta = 0.5$ (implicit Crank–Nicolson scheme)

There are two common ways to assign the boundary conditions for the heat-conduction problem. One is to maintain a constant temperature right at the polymer–mold interface, while the other is to maintain a constant temperature at the mold-cooling channels. Although the former is the simplest, it is also the least realistic. With the initial melt temperature given and the boundary temperature assigned, the numerical iteration provides the temperature distribution inside the molded article at different elapsed times.

A polystyrene plate with dimensions of 50 × 50 × 2.6 mm was examined and modeled. Here, a 2-D heat conduction model is used to simulate the 3-D geometry. Figure 1 shows schematically the description of the thermal boundary conditions and the mesh density used. During the numerical cooling analysis of the injection-molding process, it was assumed that the temperatures at the cooling channels remained fixed. Other boundary regions were assumed adiabatic for the following reasons: (1) The heat flux due to free convection between the mold and the atmosphere is relatively small and is thus neglected; (2) insulation boards placed between the mold and the platens of the machine will greatly diminish the heat flux across these interfaces; (3) the heat flux along the normal direction at the edges of the plate is relatively small compared to the heat flux normal to the faces of plate (due to the relative dimensions of the plate), and (4) geometric symmetries cause the temperature gradient to be zero along certain planes. During the heat-transfer analysis, the heavy line in Figure 1(b) represented an adiabatic boundary while the circles marked as "cooling lines" were held at fixed temperatures. A 2-D eight-noded quadratic finite element was used in the numerical scheme. The thermophysical properties representative of a polystyrene are shown in Table I. Since there is no crystallization in an amorphous polymer and also because the difference between the thermophysical properties of the liquid and solid polymer is relatively small, the properties used in the analysis were treated as constants during the heat-transfer analysis. Besides, since the heat flux across the normal direction at the plate's edges is negligible, the mold beyond the edge of the plate is neglected during the analysis. With constant cooling line temperatures along one side set at 60°C and along the other side set at 50°C, and with an initial melt temperature of 230°C within the mold, the transient heat-conduction analysis was carried out for the 2.6 mm-thick part. The calculated temperature profile across the "$c - c$" cross section of the part [see Fig. 1(b)] is shown in Figure 2. Figure 3(a) and (b) show the magnified temperature profiles within the polymer at the polymer–mold interfaces. It is not difficult to see from these graphs that the interface temperatures at the boundaries are not constant, but instead they increase with time. Also note that at 12 s after the onset of the mold-cooling simulation the mold was "opened" and the part was "ejected" and exposed to the environmental room temperature. There is a free convection heat-transfer between the polymeric part and the surrounding air. The calculations of the part's temperature then follows:

$$([C] + \Theta\Delta t[K])\{T\}^{t+\Delta t} = ([C] - (1-\Theta)\Delta t[K])\{T\}^{t} + [S]\Delta t \tag{27}$$

with

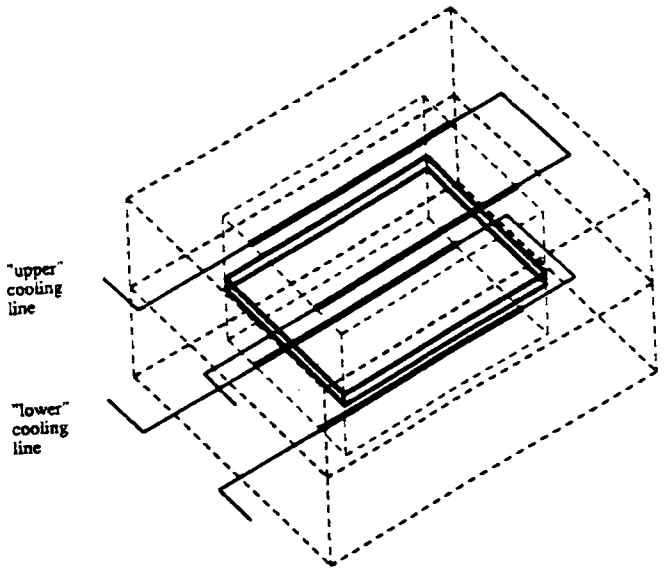

(a)

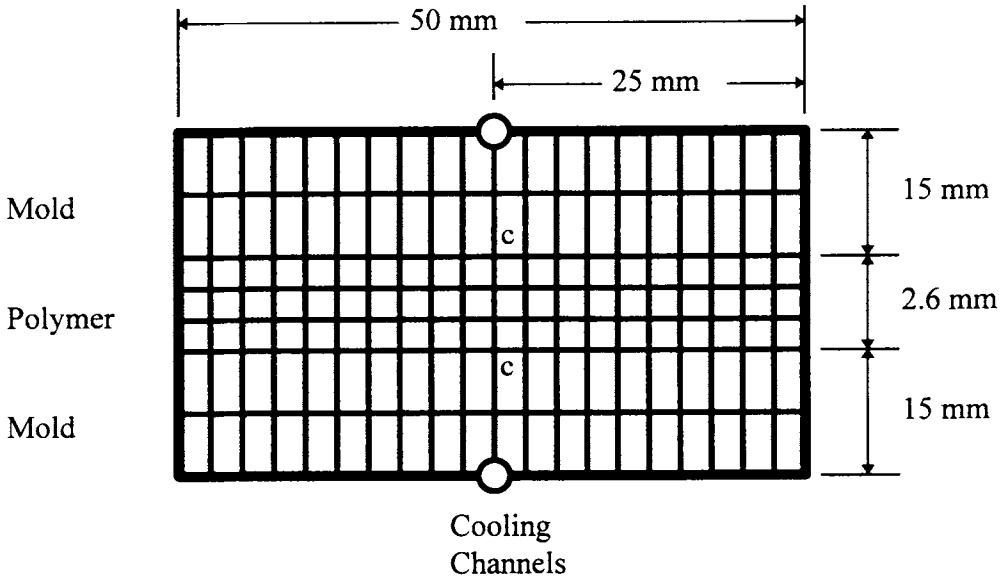

(b)

Figure 1 (a) Schematically, the injection-molded plate and the molds for analysis; (b) the plate in (a) was modeled by a 2-D finite element mesh.

Table I Material Properties of a Polystyrene[46] Used for the Numerical Simulation of Viscoelastic Phase-transformation Analysis

Elastic modules	2.4×10^9 Pa
Poisson's ratio of polymer solid	0.35
Poisson's ratio of polymer melt	0.49
Heat conductivity k	0.13 J/s m°C
Density ρ	1150 kg/m^3
Heat capacity C_p	1844 J/kg°C
Thermal expansion coefficient	70×10^{-6} m/m°C
Glass transition temperature	100°C

$$[S] = \int_S [N]^T h(\{T_{\text{room}}\} - \{T\})dS$$

where the $[S]$ term is the heat flux across the parts' surface and h is the heat-convection coefficient. These temperature profile calculations will be used later in a 2-D viscoelastic phase-transformation model that simulates the thermally induced stress of an injection-molded amorphous polymer.

RHEOLOGICAL PROPERTIES OF THERMOPLASTIC MATERIAL

The time- and temperature-dependent constitutive equation of a polystyrene was needed for the subsequent finite element analysis, so that the residual stress of a polymer plate including viscoelastic and phase transformation effects could be simulated. Stress-relaxation experiments of polystyrene, carried out by Maxwell and Rahm,[47] were used to evaluate the three parameters of the standard linear solid model. The analytical equation that describes the standard linear solid model is given by

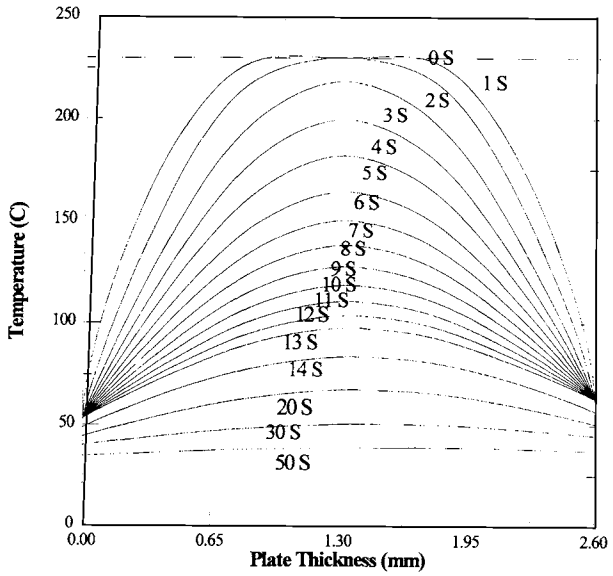

Figure 2 Temperature distribution across plate thickness "a–a" in Figure 1 as a function of cooling time with an initial polymer temperature of 230°C and cooling line temperature of 50 and 60°C (lines are the cubic spline curve fitting).

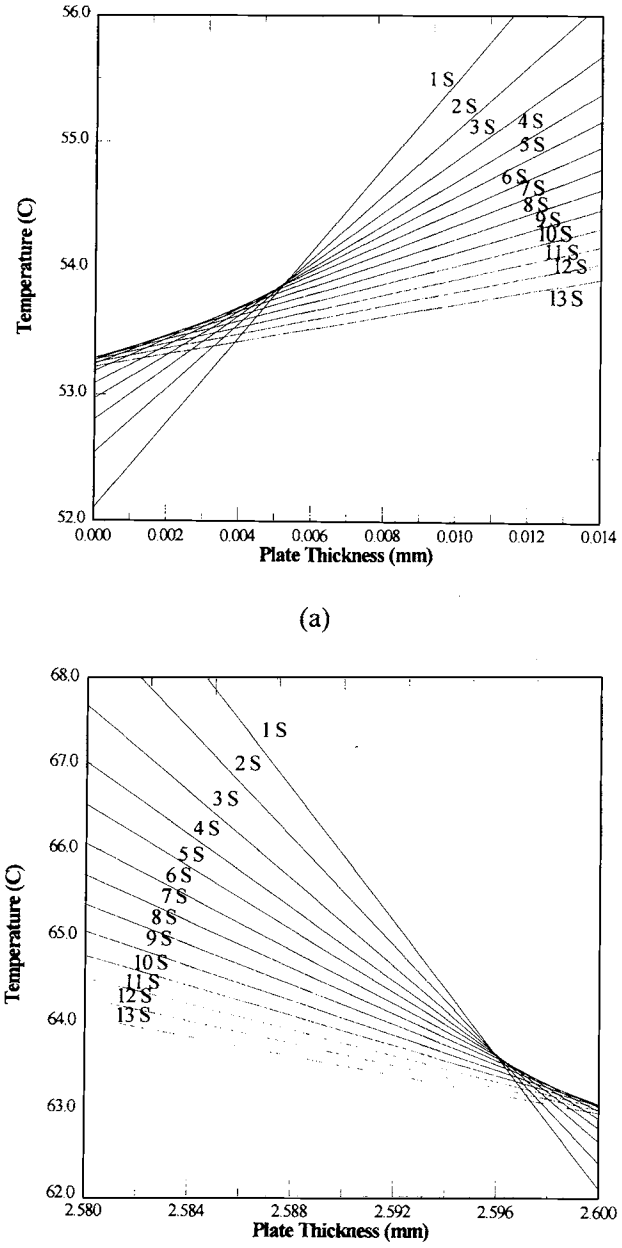

(a)

(b)

Figure 3 Temperature distribution with the plate at the polymer–mold interface.

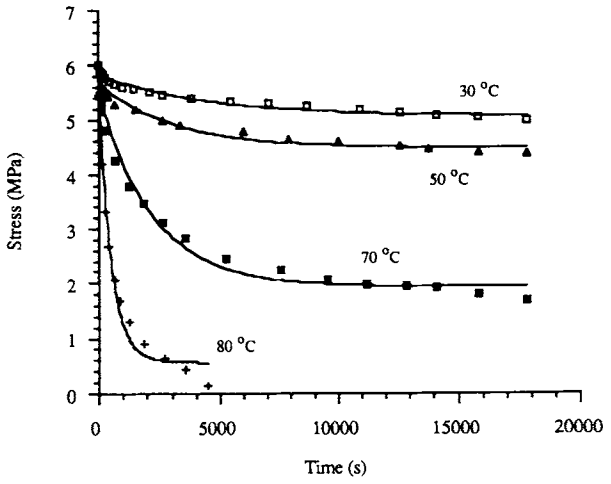

Figure 4 Curve fittings of the empirical stress relaxation data for polystyrene from Maxwell and Rahm[47] at several different temperatures.

$$\sigma_0 = E_2\varepsilon_0 + E_1\varepsilon_0 e^{(-E_1 t/\eta)} \tag{28}$$

and three material parameters (elastic modules E_1 and E_2 and viscosity η) establish the viscoelastic response of the model. By curve fitting the data of Maxwell and Rahm, the time- and temperature-dependent rheological properties of polystyrene were determined. The curve-fitting results of the stress-relaxation data for polystyrene from 30 to 80°C are shown in Figure 4. The temperature dependence of E_1 and E_2 was then fit to a second-order expression, and η was fit to a fourth-order expression:

$$E_1 = 1.17 - 5.31 \times 10^{-2}T + 8.00 \times 10^{-4}T^2 \tag{29a}$$

$$E_2 = 1.33 + 4.73 \times 10^{-2}T - 8.00 \times 10^{-4}T^2 \tag{29b}$$

$$\eta = -33.74 + 3.22 \times 10^{-1}T - 1.07 \times 10^{-1}T^2 + 1.50 \times 10^{-3}T^3 - 7.56 \times 10^{-6}T^4 \tag{29c}$$

During the injection-molding process, the residual stresses may originate from flow-induced effects and thermally induced stress. However, the latter will typically far outweigh the former for small injection-molding parts.[32] Here, the flow-induced stresses were also neglected because of its relatively small contribution; hence, for any material in the liquid state, the material models were set to respond with fluidlike behavior, i.e., any stresses in the fluid state would relax to zero very rapidly. A linear interpolation was then made to obtain the material properties (E_1, E_2, and η) of the polystyrene at temperatures within the liquid-to-solid transition region (80–120°C, which was 20°C with respect to T_g = 100°C). Although the exact temperature interval for the transition region is somewhat arbitrary, it was chosen by inspecting a typical transition interval characteristic of the modulus vs. temperature behavior for polystyrene.[7] In addition to the material parameters E_1, E_2, and η, the other material parameters used in the viscoelastic phase-transformation analysis are listed in Table I.

The relaxation modulus $G(t)$ of the standard linear solid model is defined by the following:

$$G(t) = \frac{\sigma(t)}{\varepsilon_0} = E_2 + E_1 e^{-E_1 t/\eta} \tag{30}$$

Using eq. (30) and the E_1, E_2, and η values from eq. (29), the relaxation modulus of the standard linear solid model over the temperature interval 30–80°C can be calculated, which has been carried out in Figure 5.

RESULTS FROM VISCOELASTIC PHASE-TRANSFORMATION MODEL

The numerical simulation examined the viscoelastic phase-transformation model using a 2-D overlay finite element scheme. The flowchart of the numerical scheme is shown in Figure 6. Before the application of the viscoelastic phase-transformation model, a transient heat-transfer analysis was first run to determine the temperature profiles of the polymer at different times and the transient position of the solid–liquid interface. Then, the solidified polymer was modeled as a standard linear solid by using the

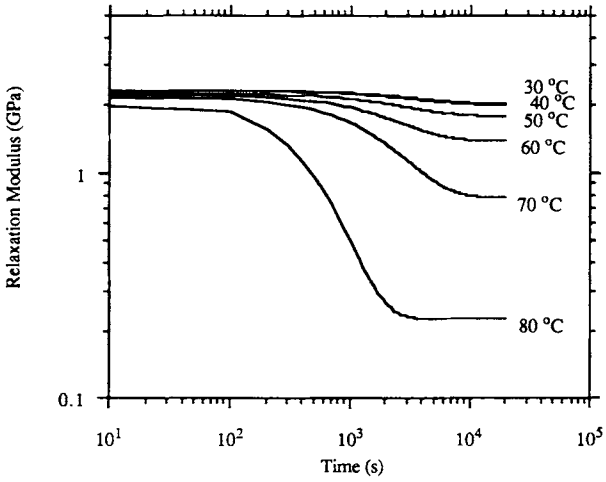

Figure 5 The relaxation modules of the standard linear solid material model to describe the behavior of solidified polymer over the temperature range from 30 to 80°C.

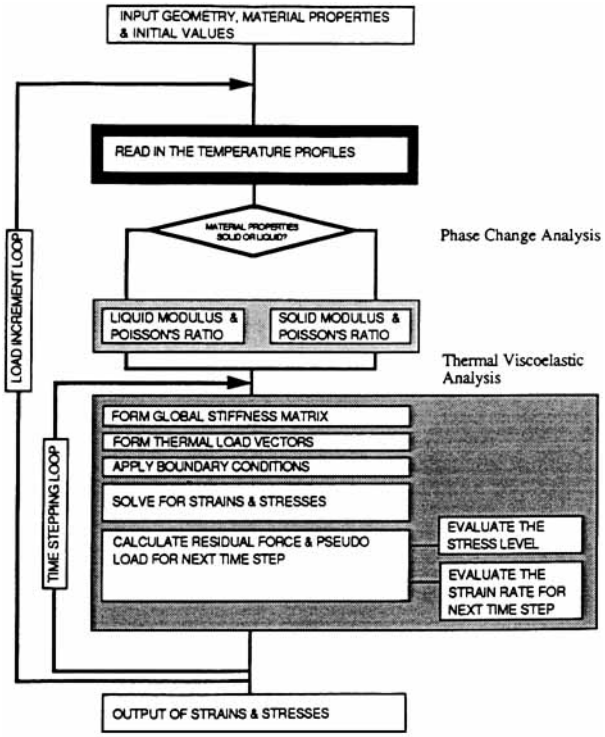

Figure 6 Flowchart for the numerical scheme of the viscoelastic phase transformation model.

overlay scheme as explained earlier, while the liquid was modeled as a viscous fluid.

To cross reference the validity of the viscoelastic phase-transformation model, the numerical results from the viscoelastic phase-transformation model were compared with experimental residual stress data for a polystyrene plate obtained by Isayev and Crouthmel[7] using a layer-removal technique. A polystyrene plate with a dimension of $50 \times 50 \times 2.6$ mm was quenched from 150 to 23°C during their experiments. The viscoelastic phase-transformation model was used to calculate the residual stress profile within the quenched polystyrene plate and compared to the empirical data by Isayev and Crouthmel. Constant temperatures were assumed at the polymer–water interface as the thermal boundary conditions for the quenching. The numerical results are shown in Figure 7. The dashed lines were the predicted values for 90 min after quenching and for 14 days after quenching. The solid lines in Figure 7 are the corresponding measured experimental data.

There are at least three factors that might affect the agreement between the numerical and experimental results shown in Figure 7. The first one is that the experimental data obtained by Isayev and Crouthmel were run with one kind of polystyrene while the material parameters (E_1, E_2, and η) used for the numerical work were obtained from the data of Maxwell and Rahm for a different polystyrene. Although both samples used in these experiments were polystyrene, different polystyrene samples may not have identical material properties. Second, the viscoelastic model used here to simulate the residual stress of the polymeric plate is a linear one; however, in reality, a polymeric material tends to exhibit nonlinear viscoelastic properties. Hence, the agreement appears to be less at longer times as can be seen in Figure 7. A possible third factor affecting the agreement pertains to the actual thermal boundary conditions used in the experimental and numerical studies. Experimentally, the polymer plate was quenched from an initial high temperature (150°C) into a low-temperature water bath (23°C); thus, the heat transfer between the part and the water during the quench process is governed by convective mechanisms. Numerically, the heat transfer at the polymer–water interface was modeled as a transient heat-conduction problem. The simulated cooling rates were higher than the actual cooling rates, which may explain why the numerical results overpredict the experimental results, i.e., less time for stress relaxation. However, when compared to the experimental data, both the Indenbom and LRW models[7] seem to overpredict the experimentally obtained residual stresses more than the viscoelastic phase-transformation model proposed in this article as shown in Figure 8.

The results further testify to the validity of the current viscoelastic phase-transformation model for

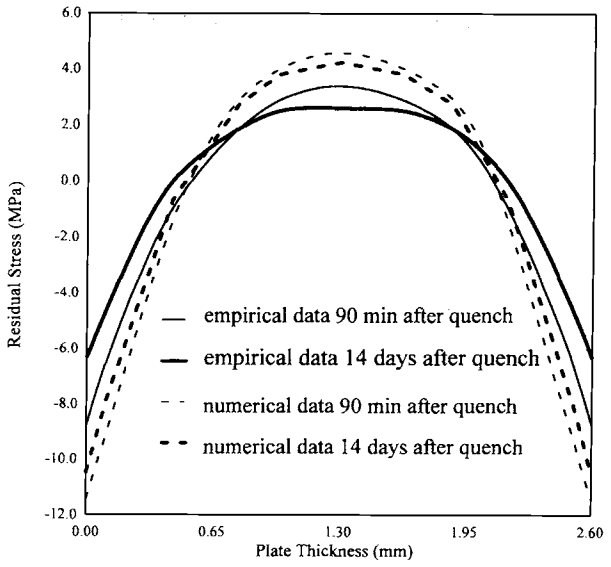

Figure 7 Comparison of the numerical results from the viscoelastic-phase transformation model with the experimental data from Isayev and Crouthmel.

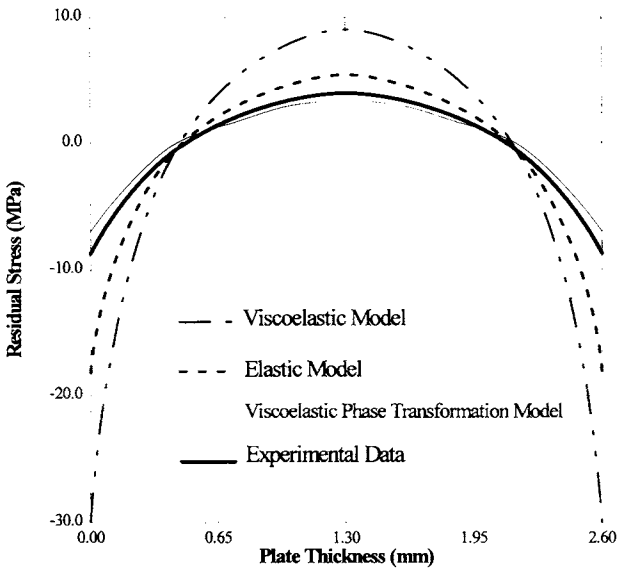

Figure 8 Comparison of Indenbom's elastic model, LRW's viscoelastic model, and the current viscoelastic phase-transformation model with the experimental data.

the prediction of injection-molding residual stresses. The effect of a different quenching history on the predicted residual stress profiles was also numerically examined through the viscoelastic phase-transformation model. Relative to the first quench condition, where the initial temperature of the plate (150°C) was suddenly quenched to a 23°C cooling bath, a second quench condition was applied in two steps, from 150°C to a 80°C cooling bath for 10 s followed by the 23°C cooling bath. The third quenching history is to cool the part from 150 to 80°C for 20 s followed by the 23°C quenching. A comparison of the predicted residual stress profiles is shown in Figure 9. From Figure 9, it can be seen that the stress profile due to the direct quench (150–23°C) had the least time to relax the residual stress profile, while in the third quenching history, one kept the materials within a higher-temperature environment for the longest time and, hence, the predicted stress profile was able to relax most. This further demonstrates that the current viscoelastic phase-transformation model can be used to capture the stress-relaxation behavior of polymers.

One of the applications of residual stress simulation is to predict the warpages in injection-molded parts. The warpage of a plastic product can be seen as primarily due to nonuniform differential shrinkages within the product which leads to the development of uneven residual stresses within the product. Relatively higher compressive stresses develop on the initially warmer side of the plate, thus causing the flat plate to bend (warp) toward the higher-temperature direction. Here, a final numerical simulation was conducted to compare the behavior of four different material models in predicting the warpage: linear elastic model, elastic phase-transformation model, and viscoelastic model proposed by other researchers[48–52] and current viscoelastic phase-transformation model. The solid-state material property of $E = 2.4 \times 10^9$ Pa and $\upsilon = 0.35$ (Ref. 46) was used for the linear elastic model, while the material properties for E_1, E_2, and η in eq. (29) and the other properties listed in Table I were used for the other models. For simulations, the plate was assumed to be cooled through channels with the "upper" channels held at a temperature of 60°C and the "lower" channels at 50°C as discussed earlier. Due to the unbalanced temperature gradient with the warmer side on "top," an unbalanced residual stress profile across the thickness will be obtained right before the opening of the molds. The residual stress profile, before the mold's opening, from the current viscoelastic phase-transformation model is shown in Figure 10. Figure 11 contains the warpage comparisons for all four of the different models: elastic model, elastic phase-transformation model, viscoelastic model, and viscoelastic phase-transformation model at 14 days. From the calculations, we can conclude that the inclusion of the phase transfor-

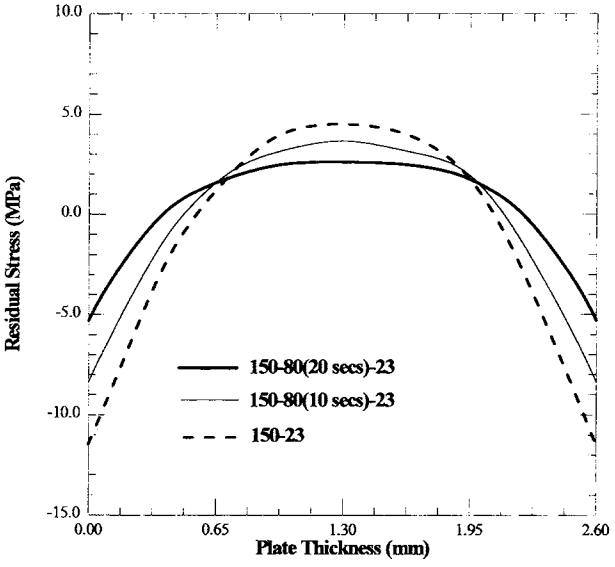

Figure 9 Residual stress profile comparison for different quenching history: (1) 150–23°C directly; (2) 150–80°C for 10 s, followed by 23°C quenching; (3) 150–80°C for 20 s, followed by 23°C quenching.

mation and the stress relaxation results in a prediction of less warpage relative to the other models, i.e., the other models overpredict the injection-molding warpages.

SUMMARY AND CONCLUSIONS

Numerical simulation of an injection-molding residual stress problem can be used to guide corrective measures if the problem arises and to prevent a potential problem from occurring in the first place. Realistic problems are, however extremely, difficult to model if one has to simultaneously account for material and geometric intricacies, which is the case for injection-molded plastics. As a minimum, the numerical modeling of thermally induced stress within injection-molded thermoplastics should not neglect the liquid-to-solid phase transformation and the stress relaxation that occurs inside the mold cavity during the cooling stage of the injection-molding cycle. This study in this article has examined the injection-molding residual stress problem from a material, geometric, and time-dependent perspective using a new material description (viscoelastic behavior including the liquid-to-solid phase transformation) with the intent of either reaching or understanding more inclusive or realistic problems. The numerical method utilized an overlay finite element scheme

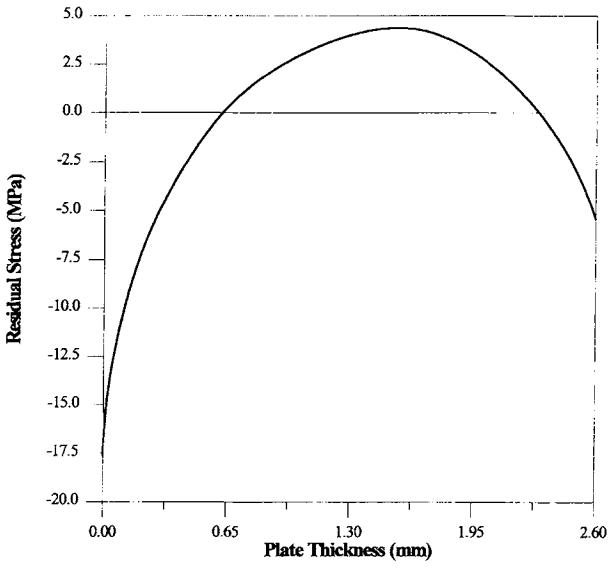

Figure 10 Numerical result of the unbalanced residual stress profile from the viscoelastic phase-transformation model, before the opening of the mold.

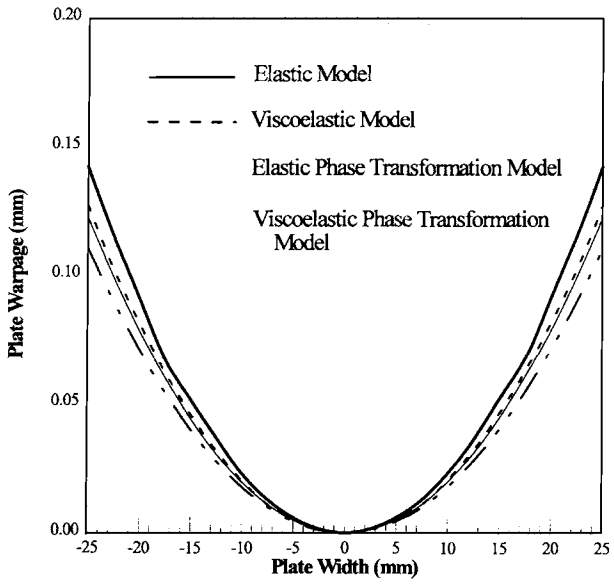

Figure 11 Comparison of the predicted warpage using four different material models: linear elastic, elastic phase transformation, viscoelastic and viscoelastic phase transformation at 14 days after the part's ejection.

to predict and simulate part deformation caused by thermally induced residual stresses. A 2-D viscoelastic phase-transformation model, using a standard linear solid for the solidified polymer and a viscous fluid model for the polymer melt, was successfully used to simulate the residual stresses and warpages of an injection-molded part. The simulation revealed that the stress-relaxation effect of the polymer should not be neglected and the liquid-to-solid phase transformation behavior should also not be neglected.

The studies here can be improved upon in the future by including the following considerations: (a) incorporating a possible yielding effect due to the high thermal stresses within the part at the moment of solidification; (b) extending the material behavior under investigation from amorphous polymers to semicrystalline polymers, and (c) rewriting the finite element code so that it can include the material model and a more general 3-D geometry.

NOMENCLATURE

σ	stress
ε	total strain

$\dot{\varepsilon}$	total strain rate
ε_e	elastic strain
$\dot{\varepsilon}_e$	elastic strain rate
ε_{vp}	viscoplastic strain
$\dot{\varepsilon}_{vp}$	viscoplastic strain rate
σ_y	yield stress
Φ	strain rate function
tr	trace
σ'	deviatoric stress tensor
$[K^n]$	initial stiffness matrix
f^n	equivalent nodal thermal load vector
η	viscosity
Θ	equals 0 (fully explicit) or 1 (fully implicit scheme)
T	temperature
$[D]$	material elasticity matrix
T_g	glass transition temperature
t	time
$[N]$	shape function
$[B]$	shape function derivative
d	displacement
E	elastic modulus
υ	Poisson's ratio
α	thermal expansion coefficient
ρ	material density
Cp	heat capacity
k	heat conductivity
h	heat convection coefficient
$[C]$	heat capacitance matrix
$[K]$	heat conductance matrix
$[S]$	heat flux matrix

REFERENCES

1. Z. Tadmor and C. G. Gogos, *Principles of Polymer Processing*, Wiley, New York, 1979.
2. L. E. Hornberger and K. L. Devries, *Exp. Mech.*, **27,** 94 (1987).
3. P. So and L. J. Broutman, *Polym. Eng. Sci.*, **16,** 785 (1976).
4. I. M. Cuckson, B. Haworth, G. J. Sandilands, and J. R. White, *Int. J. Polym. Mater.*, **9,** 21 (1981).
5. J. F. Mandell, K. L. Smith, and D. D. Huang, *Polym. Eng. Sci.*, **21,** 1173 (1981).
6. A. Siegmann, A. Buchman, and S. Kenig, *Polym. Eng. Sci.*, **22,** 560 (1982).
7. A. I. Isayev and D. L. Crouthamel, *Polym. Plast. Technol. Eng.*, **22,** 177 (1984).
8. M. Thompson and J. R. White, *Polym. Eng. Sci.*, **24,** 227 (1984).
9. L. E. Hornberger and K. L. DeVries, *Polym. Eng. Sci.*, **27,** 1473 (1987).
10. A. V. Iacope and J. R. White, *J. Appl. Polym. Sci.*, **33,** 577 (1987).
11. A. V. Iacope and J. R. White, *J. Appl. Polym. Sci.*, **33,** 607 (1987).
12. C. H. V. Hastenberg, P. C. Wildervanck, A. J. H. Leenen, and G. G. J. Schennink, *Polym. Eng. Sci.*, **32,** 506 (1992).
13. B. T. Thakkar, L. J. Broutman, and S. Kalpakjian, *Polym. Eng. Sci.*, **20,** 756 (1980).
14. C. S. Hindle, J. R. White, D. Dawson, and K. Thomas, *Polym. Eng. Sci.*, **32,** 157 (1992).
15. L. J. Broutman and S. M. Krishmakumar, *Polym. Eng. Sci.*, **16,** 74 (1976).
16. M. R. Kamal and V. Tan, *Polym. Eng. Sci.*, **19,** 558 (1979).
17. J. R. Saffell and A. H. Windle, *J. Appl. Polym. Sci.*, **25,** 1117 (1980).
18. C. J. Wust and D. C. Bogue, *J. Appl. Polym. Sci.*, **28,** 1931 (1983).
19. A. I. Isayev, *Polym. Eng. Sci.*, **23,** 271 (1983).
20. M. Takeshima and N. Funakoshi, *J. Appl. Polym. Sci.*, **32,** 3457 (1986).
21. R. K. Mittal and V. Rashmi, *Polym. Eng. Sci.*, **26,** 310 (1986).
22. S. Lee, J. De La Vega, and D. C. Bogue, *J. Appl. Polym. Sci.*, **31,** 2791 (1986).
23. R. K. Mittal and V. Rashmi, *J. Appl. Polym. Sci.*, **34,** 627 (1987).
24. T. W. D. Chan and L. J. Lee, *Polym. Eng. Sci.*, **29,** 163 (1989).
25. T. A. M. Flaman, *Polym. Eng. Sci.*, **33,** 193 (1993).
26. T. A. M. Flaman, *Polym. Eng. Sci.*, **33,** 202 (1993).
27. E. H. Lee and T. G. Rogers, *J. Appl. Mech.*, **30,** 127 (1963).
28. E. H. Lee, T. G. Rogers, and T. C. Woo, *J. Am. Ceram. Soc.*, **48,** 480 (1965).
29. B. D. Aggarwala and E. Saibel, *Phys. Chem. Glasses*, **2,** 137 (1961).
30. O. S. Narayanaswamy and R. Gardon, *J. Am. Ceram. Soc.*, **52,** 554 (1969).
31. S. M. Ohlberg and T. C. Woo, *Rheol. Acta*, **12,** 345 (1973).
32. L. C. E. Struik, *Polym. Eng. Sci.*, **18,** 798 (1978).
33. R. L. Frutiger and T. C. Woo, *J. Therm. Str.*, **2,** 45 (1979).
34. N. J. Mills, *J. Mater. Sci.*, **17,** 558 (1982).
35. C. E. Maneschy, Y. Miyano, M. Shimbo, and T. C. Woo, *Exp. Mech.*, **19,** 306 (1986).
36. K. K. Tamma, B. L. Dowler, and S. B. Railkar, *Polym. Eng. Sci.*, **28,** 421 (1988).
37. K. K. Tamma and S. B. Railkar, *Polym. Eng. Sci.*, **29,** 100 (1989).
38. A. Cohen and M. G. Dibbs, *J. Appl. Polym. Sci.*, **37,** 1541 (1989).
39. L. Douven, PhD Thesis, Eindhoven University of Technology, 1991.
40. M. Rezayat and R. O. Stafford, *Polym. Eng. Sci.*, **31,** 393 (1991).
41. F. P. T. Baaijens, *Rheol. Acta*, **30,** 284 (1991).
42. S.-J. Liu and J. X. Rietveld, *SPE-ANTEC Conf. Proceed.*, **40,** 684 (1995).

43. D. R. J. Owen and E. Hinton, *Finite Element in Plasticity,* Pineridge Press, Swansea, UK, 1980.
44. I. C. Cormeau, *Int. J. Num. Meth. Eng.,* **9,** 109 (1975).
45. C. J. Yu and J. E. Sunderland, *Polym. Eng. Sci.,* **32,** 191 (1992).
46. D. V. Rosato and D. V. Rosato, *Plastics Processing Data Handbook,* Van Nostrand Reinhold, New York, 1990.
47. B. Maxwell and L. F. Rahm, *Ind. Eng. Chem.,* **41,** 1988 (1949).
48. M. St. Jacques, *Polym. Eng. Sci.,* **22,** 241 (1982).
49. T. Matsuoka, J.-I. Takabatake, A. Koiwai, Y. Inoue, S. Yamamoto, and H. Takahashi, *Polym. Eng. Sci.,* **31,** 1043 (1991).
50. H. H. Chiang, K. Himasekhar, N. Santhanam, and K. K. Wang, in *ASME, Winter Conference Proceedings,* HTD-175/MD-25, 1991, p. 133.
51. K. K. Kabanemi and M. J. Crochet, *Int. Polym. Proc.,* **7,** 60 (1992).
52. D. D. Joye, *J. Appl. Polym. Sci.,* **47,** 345 (1993).
53. R. J. Crawford, *Plastics Engineering,* Pergamon Press, New York, 1987.
54. C. L. Tucker III, *Computer Modeling for Polymer Processing,* Hanser, New York, 1989.

Received December 1, 1995
Accepted June 1, 1996